第25卷第4期
2006年8月

红外与毫米波学报
J. Infrared Millim. Waves

Vol. 25, No. 4
August, 2006

文章编号:1001-9014(2006)04-0241-05

PERFORMANCE ANALYSIS OF EXTENDED WAVELENGTH InGaAs PHOTOVOLTAIC DETECTORS GROWN WITH GAS SOURCE MBE

HAO Guo-Qiang, ZHANG Yong-Gang, GU Yi, LI Ai-Zhen, ZHU Cheng
(State Key Laboratory of Functional Materials for Informatics, Shanghai Institute of Microsystem and Information Technology, Chinese Academy of Sciences, Shanghai 200050, China)

Abstract: The performance of pin $In_xGa_{1-x}As$ photovoltaic detectors with cutoff wavelengths of 1.7μm (x=0.53), 1.9μm (x=0.6) and 2.2μm (x=0.7) was investigated theoretically and experimentally. The analyses of dark current show that due to the ohmic conduction leakage current at lower reverse bias and trap assisted tunneling current at higher reverse bias, the dark currents of extended wavelength $In_{0.6}Ga_{0.4}As$ and $In_{0.7}Ga_{0.3}As$ detectors are considerable larger than that of $In_{0.53}Ga_{0.47}As$ detectors. The analyses of the dependence of R_0A product on temperature and the carrier concentration of light absorption layer show that $In_xGa_{1-x}As$ detectors can exhibit excellent performance at thermoelectric cooling temperatures and R_0A can benefit from the slightly higher doping in the light absorption layer.

Key words: optoelectronics; photodetectors; dark current analysis; temperature behavior; R_0A

CLC number: TB4 **Document code**: A

气态源分子束外延生长扩展波长InGaAs探测器性能分析

郝国强, 张永刚, 顾 溢, 李爱珍, 朱 诚
(中国科学院上海微系统与信息技术研究所 信息功能材料国家重点实验室,上海 200050)

摘要:从理论与实验两方面对截止波长为1.7μm (x=0.53), 1.9μm (x=0.6)和2.2μm (x=0.7) pin $In_xGa_{1-x}As$探测器性能进行了研究.对探测器暗电流的研究结果表明,扩展波长$In_{0.6}Ga_{0.4}As$,$In_{0.7}Ga_{0.3}As$探测器在反向偏置低压区,欧姆电流占据主导地位;在反向偏置高压区,缺陷隧穿电流占主导地位;且扩展波长$In_{0.6}Ga_{0.4}As$,$In_{0.7}Ga_{0.3}As$探测器的暗电流比$In_{0.53}Ga_{0.47}As$探测器增加较大.对探测器R_0A随温度及i层载流子浓度变化关系的研究结果表明,在热电制冷温度下探测器性能可得到较大提高,i层的轻掺杂可使探测器的R_0A得到改善.

关 键 词:光电子学;光电探测器;暗电流分析;温度特性;零偏压下微分电阻与面积乘积

Introduction

The short wavelength infrared band of 1~3 μm is becoming increasingly important for the applications in earth observation, remote sensing, night vision, temperature sensing and process control [1]. In addition to HgCdTe, PbS and antimonide materials, the ternary InGaAs can also cover part of this band. The detectors using InGaAs have better performances such as low dark current, high quantum efficiency and high detectivity because a more mature growth and processing technology can be relied on [2~4]. Dark current and zero-bias resistance-junction area product R_0A are the main parameters of concern in those detectors for high sensitivity and low noise applications, however, little attention has been given to the analysis of R_0A product of InGaAs detectors. In this work, the dark current and R_0A $In_xGa_{1-x}As$ photovoltaic detectors with cutoff

Received: 2005-11-21, **revised date**: 2006-04-17　　收稿日期: 2005-11-21, 修回日期: 2006-04-17
Foundation item: National "973" Project(G20000683), National "863" Project(2002AA313040)
Biography: HAO Guo-Qiang (1977-), male, Hebei, China, candidate for doctor degree, research area is semiconductor optoelectronic materials and devices.

wavelengths of 1.7μm, 1.9μm and 2.2μm grown by gas source molecular beam epitaxy (GSMBE) have been investigated.

The $In_xGa_{1-x}As$ detectors (with x = 0.53, 0.6 and 0.7) were grown by using GSMBE[5]. For lattice matched $In_{0.53}Ga_{0.47}As$ detectors, a p^+ − InP top layer was used. By using capacitance voltage (C-V) measurements, the carrier concentration in the absorbing layers was found to be around $1 \sim 5 \times 10^{16}\,cm^{-3}$ for each detector, which are consistent with the quite lower Si doping level during the growth. The dark currents and shunt resistances of those $In_xGa_{1-x}As$ detectors have been measured by using a HP4156A precise semiconductor analyzer. At room temperature, tens of detector chips in each wafer were measured on wafer using a probe station, and most of detector chips have quite identical characteristics except for some chips on the edge of wafer. After that, the wafers were dicing into chips, and several chips with typical characteristics in each wafer were mounted into DIP packages and installed on the cold head of a closed cycle He cryopump for temperature dependent measurement.

1 Analysis of dark current

The total reverse-biased dark current in a pin detector is composed of several parts with independent carrier transport mechanisms. The important dark current components are diffusion current, generation-recombination current, ohmic conduction leakage current, band-to-band tunneling current and trap assisted tunneling current [6~10]. For InGaAs detectors with pin mesa structure, the diffusion current from the p^+ layer can be neglected and only diffusion current from the i layer needs to be considered. Five contributions to the dark current can be expressed by:

$$I_{dif} = qn_i^2\left(\frac{D_p}{\tau_p}\right)^{1/2}\left(\frac{A}{N_d}\right)\left[\exp\left(\frac{qV}{kT}\right)-1\right] \quad , \tag{1}$$

$$I_{gr} = \frac{qn_iAW}{\tau_{eff}}\left[\exp\left(\frac{qV}{2kT}\right)-1\right] \quad , \tag{2}$$

$$I_{0hm} = \frac{-V}{R_{eff}} \quad , \tag{3}$$

$$I_t^{b-b} = \gamma A\exp\left(-\frac{\Theta m_0^{1/2}E_g^{3/2}}{q\hbar E_m}\right) \quad , \tag{4}$$

$$I_t^t = CE_mV\exp\left(-\frac{\Theta m_0^{1/2}E_g^{3/2}}{q\hbar E_m}\right) \quad , \tag{5}$$

where D_p, τ_p, and N_d are hole diffusion constant, hole lifetime and electron concentration in the i layer, τ_{eff} is effective life of minor carrier in space-charge region, A is the junction area. E_g and n_i are the energy gap and intrinsic carrier concentration of $In_xGa_{1-x}As$ (the composition dependence of E_g at 300K can be expressed by $E_g = 0.324 + 0.7(1-x) + 0.4(1-x)^2$ with a temperature coefficient of $-3\times10^{-4}\,eV/K$), where $n_i = (N_cN_v)^{1/2}\exp(-Eg/2kT)$, N_c and N_v are the effective density of states in conduction band and valence band. Depletion region width W is given by $W = [-2\varepsilon(V_b + V)/qN_d]^{1/2}$, where ε is dielectric constant of i layer and V_b is the built-in voltage. Effective resistance of the detector R_{eff} could be expressed as $R_{eff} = R_\infty \exp(\Delta E_a/KT)$, where ΔE_a is the thermal activation energy and R_∞ is a constant. For tunneling current, E_m is the junction electric field given by $E_m = -2(V + V_b)/W$, E_t is the trap tunneling barrier, C is trap tunneling constant. The parameter γ depends on the initial and final states of tunneling carrier given by $\gamma = (2m_e/E_g)^{1/2}(q^3E_mV/4\pi^2\hbar^2)$. The parameter Θ is a dimensionless quantity given by $\Theta = \alpha\,(2m_e/m_0)^{1/2}$, α depends on the detailed shape of the tunneling barrier. Other symbols are with their usual meaning.

τ_p, τ_{eff} and R_{eff} have influence on diffusion current, generation-recombination current and ohmic conduction leakage current respectively, which dominate dark current at lower bias. τ_{eff} dominates the I_{gr} and changes with composition greatly [4], whereas τ_p has only weaker influence on dark current,. In the simulation, τ_p and τ_{eff} at 300K were chosen to be 0.6ns/70ns for x = 0.53 [6,7], and 0.3ns/20ns or 0.15ns/7ns for x = 0.6 and x = 0.7 respectively. In the simulation of R_0A, the τ_{eff} and τ_p are all set to be independent of N_d[6,11]. Θ ($0.1 < \Theta < 0.5$) and C (correlated to the concentration of the mid-gap trap and increased with the cutoff wavelength of InGaAs detectors) have influence on tunneling current, which dominates the dark current at higher bias. In the simulation, those parameters are treated as adjustable parameters, and their values were extracted by the best fit of the simulation results with measured data at lower or higher bias respectively.

Table 1 The parameters for InGaAs detectors at 300K
表 1 300K 时 InGaAs 探测器参数

$In_xGa_{1-x}As$	x = 0.53	x = 0.6	x = 0.7
$ni(cm^{-3})$	6.1×10^{11}	3.3×10^{12}	1.7×10^{13}
$E_g(eV)$	0.75	0.66	0.57
m_e/m_0	0.041	0.039	0.035
$D_p(cm^2/s)$	13	14	15
$\varepsilon/\varepsilon_0$	13.9	14.0	14.3
$N_d(cm^{-3})$	5×10^{16}	2×10^{16}	1×10^{16}
$E_t(eV)$	0.16	0.16	0.16
$\tau_p(ps)$	600	300	150
$\tau_{eff}(ns)$	70	20	7
Θ	0.31	0.30	0.28
$R_{eff}(\Omega)$	5×10^9	1×10^7	1×10^6
$C(A/V^2cm)$	2×10^{-9}	4×10^{-6}	4×10^{-5}

The measured and simulated dark currents of the detectors with 150μm diameter at 300K as well as each current component for different detectors are shown in figure 1, and the parameters used in the simulation are listed in table 1. It can be seen that, the theory could fit the measured data well. In figure 1, $In_{0.53}Ga_{0.47}As$ detector has deferent current-voltage characteristic with $In_{0.6}Ga_{0.4}As$ and $In_{0.7}Ga_{0.3}As$ detectors. For $In_{0.53}Ga_{0.47}As$ detector, the dark current is dominated by the generation recombination current at lower bias and by the band-to-band tunneling current at higher bias (shown in figure 1(b)), while for $In_{0.6}Ga_{0.4}As$ and $In_{0.7}Ga_{0.3}As$ detectors, the dark currents are dominated by the ohmic conduction leakage current at lower bias and by the trap assisted tunneling current at higher bias (shown in figure 1(c), (d)).

The dark currents of $In_{0.6}Ga_{0.4}As$ and $In_{0.7}Ga_{0.3}As$ detectors are considerably larger than that of $In_{0.53}Ga_{0.47}As$ detector, especially at lower reverse bias voltage. It is because that the smaller band gap of $In_{0.6}Ga_{0.4}As$ and $In_{0.7}Ga_{0.3}As$ not only leads to an increased intrinsic carrier concentration, which affects both the diffusion and the generation recombination currents, but also leads to increasing ohmic conduction leakage current and tunneling current. Another source of the larger dark current is the exiting of defects caused by the lattice mismatch between the absorption layers ($In_{0.6}Ga_{0.4}As$ and $In_{0.7}Ga_{0.3}As$ layers) and InP substrate. These defects provide midgap generation recombination centers and trap tunneling centers, which increase the generation recombination current and the

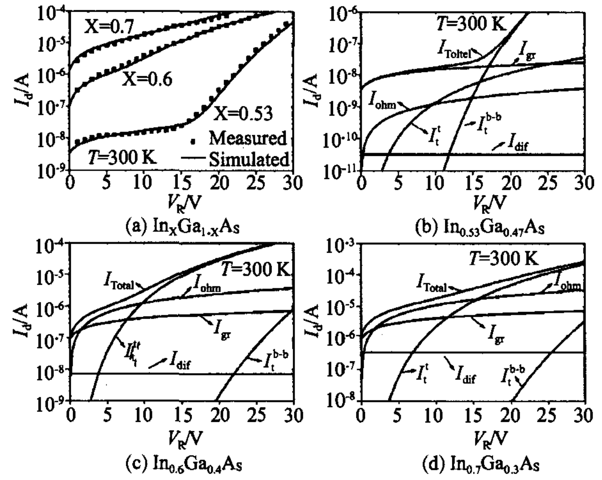

Fig. 1 Measured (dots) and simulated (lines) dark currents versus reverse bias voltage for $In_{0.53}Ga_{0.47}As$, $In_{0.6}Ga_{0.4}As$ and $In_{0.7}Ga_{0.3}As$ detectors (a) 300K (b) each component of the simulated dark currents $In_{0.53}Ga_{0.47}As$ (c) $In_{0.6}Ga_{0.4}As$ (d) $In_{0.7}Ga_{0.3}As$ detectors

图 1 (a) 300K 时 $In_{0.53}Ga_{0.47}As$, $In_{0.6}Ga_{0.4}As$ 和 $In_{0.7}Ga_{0.3}As$ 探测器暗电流随反向偏压变化关系,其中点为实测值,线为模拟值;探测器暗电流分量随反向偏压变化关系 (b) $In_{0.53}Ga_{0.47}As$ (c) $In_{0.6}Ga_{0.4}As$ (d) $In_{0.7}Ga_{0.3}As$

trap assisted tunneling current respectively. Therefore reducing defects is important for improving the performance of extended wavelength InGaAs detectors. The $In_xGa_{1-x}As$ detectors (x = 0.53, 0.6 and 0.7) with different diameters (50μm, 100μm, 150μm) have been measured at 300K, a quite linear dependence of dark current on the junction area could be deduced, which indicates that the dark current is mainly dominated by the bulk generation, not the surface generation.

2 Analysis of R_0A

R_0A product is a figure of merit commonly used to characterize infrared photovoltaic detector. The R_0A product is determined by various noise mechanisms caused by diffusion, generation-recombination, ohmic, band-to-band tunneling and trap assisted tunneling currents [11,12]. For pin mesa structure InGaAs detectors, five R_0A product components are given by:

$$R_0A_{dif} = \frac{kT}{q^2}\frac{L_pN_d}{D_pn_i^2}\frac{\cosh\left(\frac{d-W}{L_p}\right)}{\sinh\left(\frac{d-W}{L_p}\right)} \quad , \qquad (6)$$

$$R_0A_{gr}=\frac{V_b\tau_{eff}}{qWn_i}\quad, \tag{7}$$

$$R_0A_{ohm}=R_{eff}A\quad, \tag{8}$$

$$R_0A_t^{b-b}=\left[\left(\frac{2m_e}{E_g}\right)^{\frac{1}{2}}\frac{q^3E_m}{4\pi^2\hbar^2}\exp\left(-\frac{\Theta m_0^{1/2}E_g^{3/2}}{q\hbar E_m}\right)\right]^{-1}\quad, \tag{9}$$

$$R_0A_t^t=\left[CE_m\exp\left(-\frac{\Theta m_0^{1/2}E_t^{3/2}}{q\hbar E_m}\right)\right]^{-1}\quad, \tag{10}$$

where d is the width of i layer and L_p is hole diffusion length, $L_p=(D_p\tau_p)^{1/2}$. Because all the noise mechanisms are almost independent, R_0A_{Total} can be expressed by

$$\frac{1}{R_0A_{Total}}=\frac{1}{R_0A_{dif}}+\frac{1}{R_0A_{gr}}+\frac{1}{R_0A_{ohm}}+\frac{1}{R_0A_t^{b-b}}+\frac{1}{R_0A_t^t}\quad. \tag{11}$$

From equations (6) to (10), we can find that the temperature and the carrier concentration of i layer N_d have larger influence on R_0A product. Therefore, in the following we pay much attention to the dependence of R_0A product on temperature and N_d.

Figure 2 shows the temperature behavior of the measured and simulated R_0A product of the detectors with 150μm diameter. It could be observed that the theory may also fit measured data well. The temperature dependence of R_0A_{dif} and R_0A_{gr} for $In_{0.7}Ga_{0.3}As$ detectors are also shown in figure 2 (dash lines).

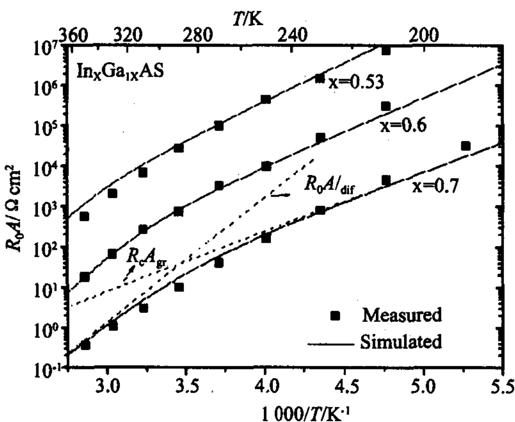

Fig. 2 Measured (dots) and simulated (lines) R_0A products of In_xGa_{1-x} As detectors at different temperatures (R_0A_{dif} and R_0A_{gr} of $In_{0.7}Ga_{0.3}As$ detector is also shown (dash line).)

图2 $In_xGa_{1-x}As$ 探测器 R_0A 随温度变化关系,点为实测值,线为模拟值(图中虚线给出了 $In_{0.7}Ga_{0.3}As$ 探测器 R_0A_{dif} 和 R_0A_{gr} 随温度的变化关系)

From figure 2, we can see that both R_0A_{dif} and R_0A_{gr} have contributions to R_0A_{Total} at higher temperature, while at lower temperature R_0A_{Total} is dominated by R_0A_{gr}. The temperature dependence of R_0A product of $In_{0.53}Ga_{0.47}As$ and $In_{0.6}Ga_{0.4}As$ detectors has similar characteristics, however, the cross over temperature increases with the decreasing of cutoff wavelength, because the smaller band gap of InGaAs leads to the increasing of diffusion current ($I_{dif}\propto n_i^2\propto\exp(-E_g/kT)$).

R_0A product is directly correlated to the peak detectivity expressed by $D_\lambda^*=(\lambda/2hc)\eta q(R_0A/kT)^{1/2}$, where λ is peak response wavelength, c is light velocity and η is quantum efficiency. Using the measured R_0A products, the peak detectivities $D^*\lambda$ at three temperatures have been calculated. In the calculation, the peak response wavelengths of $In_{0.53}Ga_{0.47}As$, $In_{0.6}Ga_{0.4}As$ and $In_{0.7}Ga_{0.3}As$ detectors are 1.65μm, 1.86μm and 2.13μm respectively and quantum efficiency η is supposed to be 0.7. Table 2 shows the measured R_0A products and corresponding peak detectivities. It can be seen from table 2 that, when temperatures decrease from 290K to 210K, R_0A products increases more than two orders of magnitude and corresponding peak detectivities increases more than an order of magnitude, so those $In_xGa_{1-x}As$ detectors could exhibit excellent performance at TE (thermoelectric) cooling temperatures.

R_0A_{Total} and each R_0A product components versus N_d at 300K also have been plotted as shown in figure 3. It can be seen that in lower carrier concentration, R_0A_{gr} makes major contribution to R_0A_{Total} for $In_{0.53}Ga_{0.47}As$ detector (as shown in figure 3 (a)), while for $In_{0.6}Ga_{0.4}As$ and $In_{0.7}Ga_{0.3}As$ detectors both R_0A_{dif}

Table 2 Measured R_0A product and corresponding peak detectivity (supposing quantum efficiency η is 0.7) of fabricated $In_xGa_{1-x}As$ detectors at various temperatures

表2 在不同温度下 InGaAs 探测器 R_0A 测量值及 D_λ^* (假设探测器量子效率为 0.7)

	T=350K		T=290K		T=210K	
$In_xGa_{1-x}As$	R_0A (Ωcm^2)	$D*\lambda$ ($cmHz^{1/2}/W$)	R_0A (Ωcm^2)	D_λ^* ($cmHz^{1/2}/W$)	R_0A (Ωcm^2)	D_λ^* ($cmHz^{1/2}/W$)
x=0.53	565	1.59×10^{11}	2.81×10^4	1.23×10^{12}	7.56×10^6	2.2×10^{13}
x=0.6	18.8	3.27×10^{10}	766	2.30×10^{11}	3.18×10^5	5.49×10^{12}
x=0.7	0.40	5.45×10^9	10.3	3.05×10^{10}	4.69×10^3	7.65×10^{11}

and R_0A_{gr} have contributions to R_0A_{Total} (as shown in figure 3 (b), (c)). R_0A_{Total} only increase slightly with the increasing of N_d because of $R_0A_{dif} \propto N_d$ in equation (6) and $R_0A_{gr} \propto N_d^{1/2}$ in equation (7). However, due to the effect of $R_0A_t^t$, R_0A_{Total} reaches maximal value and then drops sharply with the increasing of N_d ($R_0A_t^t \propto N_d^{-1/2}\exp(N_d^{-1/2})$). This indicates that R_0A_{Total} can benefit from the slightly higher doping in the i layer and if the trap assisted tunneling current reduced, R_0A_{Total} may increase further.

We compare the dependence of R_0A_{Total} on N_d for different $In_xGa_{1-x}As$ detectors as shown in figure 3 (d). It can be seen that those different $In_xGa_{1-x}As$ detectors have similar characteristics. However, with the increase of x, the N_d at maximal R_0A_{Total} decreases (when x increases from 0.53 to 0.7, N_d at maximal R_0A_{Total} decreases from $5\times10^{16}cm^{-3}$ to $2\times10^{16}cm^{-3}$), which is due to the larger trap assisted tunneling current of extended wavelength $In_{0.6}Ga_{0.4}As$ and $In_{0.7}Ga_{0.3}As$ detectors.

3 Conclusions

In conclusion, for $In_{0.53}Ga_{0.47}As$ detector the dark current is dominated by generation-recombination current at lower reverse bias and band to band tunneling current at higher reverse bias, while for $In_{0.6}Ga_{0.4}As$ and $In_{0.7}Ga_{0.3}As$ detectors, the dark currents are dominated by ohmic conduction leakage current and trap assisted tunneling current. At higher temperature both diffusion and generation-recombination mechanisms have contributions to the noise; while at lower temperature generation-recombination mechanism becomes dominant. In addition, R_0A can benefit from the slightly higher doping in the i layer, even though higher dark current occurs at higher bias, and this is quite important for the photovoltaic detectors working at zero bias.

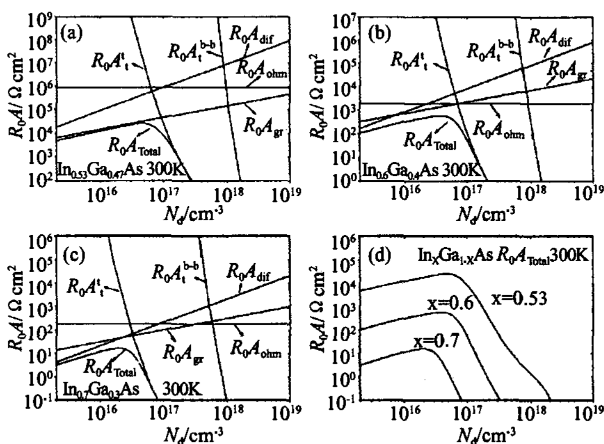

Fig. 3 Dependence of R_0A_{Total} and R_0A product components on carrier concentration of i layer at 300K for (a): $In_{0.53}Ga_{0.47}As$, (b): $In_{0.6}Ga_{0.4}As$ and (c): $In_{0.7}Ga_{0.3}As$ detectors; the comparison of R_0A_{Total} is also shown in (d).

图3 300K时R_0A_{Total}和R_0A分量随i层载流子浓度的变化关系(a) $In_{0.53}Ga_{0.47}As$, (b) $In_{0.6}Ga_{0.4}As$, (c) $In_{0.7}Ga_{0.3}As$, (d) $In_xGa_{1-x}As$(x=0.53, 0.6, 0.7)探测器R_0A_{Total}比较

REFERENCES

[1] Linga K R, Olsen G H, Ban V S, *et al.* Dark current analysis and characterization of $Ga_{1-x}In_xAs/InAs_yP_{1-y}$ graded photodiodes with x > 0.53 for response to longer wavelengths (>1.7(m)) [J]. *IEEE J. Lightwave Technol.*, 1992, **10**: 1050—1055.

[2] Rogalski A. Infrared detectors: status and trends [J]. *Progress in Quantum Electron.*, 2003, **27**: 59—210.

[3] Ettenberg M H, Lange M J, O' Grady M T, *et al.* A room temperature 640 × 512 pixel near-infrared InGaAs focal plane array [J]. *Proceedings of SPIE*, 2000, **4028**: 201—207.

[4] Kim D, Forrest S R. A three wavelength infrared focal plane array detector element [J]. *IEEE Photon. Technol. Lett.*, 1994, **6**: 235—238.

[5] ZHANG Yong-Gang, GU Yi, ZHU Cheng, *et al.* Fabrication of short wavelength infrared InGaAs/InP photovoltaic detector series [J]. *J. Infrared Millim. Waves* (张永刚,顾溢,朱诚,等. 短波红外 InGaAs/InP 光伏探测器系列的研制. 红外与毫米波学报), 2006, **25**(1): 6—9.

[6] Forrest S R. Performance of $In_xGa_{1-x}As_yP_{1-y}$ photodiodes with dark current limited by diffusion, generation recombination, and tunneling [J]. *IEEE J. Quantum Electron.*, 1981, **17**: 217—226.

[7] Forrest S R, Leheny R F, Nahory R E, *et al.* $In_{0.53}Ga_{0.47}As$ photodiodes with dark current limited by generation-recombination and tunneling [J]. *Appl. Phys. Lett.*, 1980, **37**: 322—325.

[8] Kim O K, Dutt B V. A low dark-current planar InGaAs p-i-n photodiode with a quaternary InGaAsP cap layer [J]. *IEEE J. Quantum Electron.*, 1985, **QE-21**: 138—143.

[9] Trommer R, Albrecht H. Confirmation of tunneling current via traps by DLTS measurements in InGaAs photodiodes [J]. *Jpn. J. Appl. Phys.*, 1983, **22**: L364—L366.

[10] Philippe P, Poulain P, Kazmierski K, *et al.* Dark-current and capacitance analysis of InGaAs/InP photodiodes grown by metalorganic chemical vapor deposition [J]. *J. Appl. Phys.*, 1986, **59**: 1771—1773.

[11] Tian Y, Zhou T, Zhang B, *et al.* Recombination lifetime of $In_{0.53}Ga_{0.47}As$ as a function of doping density [J]. *J. Phys. D: Appl. Phys.*, 1998, **31**: 3291—3297.

[12] Rogalski A. *Infrared Photon Detectors* [M]. Washington, USA: SPIE optical engineering press, 1995. 5—30.